Proceedings of IMECE'03
2003 ASME International Mechanical Engineering Congress & Exposition
Washington, D.C., November 16-21, 2003

IMECE2003/NCA-43696

RECENT IMPROVEMENTS OF THE ALGORITHM OF MODE ISOLATION

Jerry H. Ginsberg and Matthew S. Allen
The Woodruff School of Mechanical Engineering
Georgia Institute of Technology Atlanta, GA 30332-0405
jerry.ginsberg@me.gatech.edu

ABSTRACT

The Algorithm of Mode Isolation (AMI) identifies the natural frequencies, modal damping ratios, and mode vectors of a system by processing complex frequency response data. It uses an iterative procedure based on the fact that a general frequency response function is a superposition of modal contributions. The iterations focus successively on a single mode. The mode that is in focus is isolated by subtracting the other modal contributions using prior estimates of their modal properties. This process leads to a self-contained identification of the number of modes that participate in any frequency band, whereas other techniques require a priori guesses. This paper describes modifications intended to improve AMI's accuracy and reduce its computational effort. These involve the use of a new linear least squares method for identifying the natural frequency and damping ratio of a single mode, and a linear least squares global fit of the data in order to identify mode vectors. Results are presented for a model of a cantilever beam with suspended spring-mass-dashpot systems. This system was used by Drexel, Ginsberg, and Zaki [Journal of Vibration and Acoustics, 2003 (forthcoming)] to assess the prior version's ability to identify weakly excited modes and modes having close natural frequencies in the presence of high noise levels. Application of the modified version of AMI to the same system is shown to lead to significantly more accurate damping ratios and mode vectors, with equally good natural frequencies.

KEYWORDS:

Experimental modal analysis, system identification.

NOMENCLATURE

$A_{jk}^{(1)}, A_{jk}^{(2)}$	Modal displacement factors
$G_{jP}(\omega)$	Displacement transfer function
$G_{jPk}(\omega)$	kth mode's contribution to $G_{jP}(\omega)$
Q_j	Generalized force amplitudes
$\{q\}$	Generalized coordinates
Ψ_n	Ritz series basis functions
w	Transverse displacement
$X^{(k)}(\omega)$, $Y^{(k-1)}(\omega)$	Frequency domain data used to identify the kth mode
$y_j(t_n)$	Time domain impulse responses
ζ_k	kth modal damping ratio
λ_k	kth eigenvalue
ω_k	kth natural frequency
ω	Drive frequency
$\{\Phi_k\}$	Mass-normalized mode vectors

INTRODUCTION

Most experimental modal analysis algorithms in current use try to identify all modal parameters simultaneously, creating a need to estimate in advance the number of modes on which the "best fit" model will be constructed. Typically, the number of modes is over-estimated, then the redundant modes are truncated. Most methods identify the correct model order via singular value decomposition and/or stabilization diagrams, which display eigenvalues obtained from a range of guesses for the system order. Even then, it can be difficult to determine the true order of the system and to distinguish the true modes of the system from computational modes. For example, Doebling, Alvin and Peterson [1], working with the Eigensystem Realization Algorithm, showed that not only might overestimating the number of modes raise the computational effort, but it can also lead to false estimations and numerical instability.

Previous papers have indicated that the Algorithm of Mode Isolation (AMI) offers a promising alternative. The algorithm was initially described by Drexel and Ginsberg [2]

for classical, undamped, modal analysis. The algorithm was then extended to modal analysis in the state space in order to account for arbitrary damping (Drexel and Ginsberg [3], Drexel, Ginsberg, and Zaki [4]). Subsequent to these basic developments, an improvement implemented by Zaki [5] and Zaki and Ginsberg [6] was to use the original AMI concept to identify the eigenvalues, after which the mode vectors are obtained from a linear least-squares global fit to all frequency response functions (FRF). The concept of separating evaluation of eigenvalues and mode vectors is contained in the procedure described by Balmes [7], which iterates between the poles and residues of complex frequency response functions (FRF). In the present context one would expect it to provide more accurate results for mass-normalized mode vectors, especially in cases where the drive point mobility of a mode is weak. A different aspect of AMI was addressed by Ginsberg, Allen, and Ferri [8], who introduced a linear least squares algorithm for fitting the resonant peak of an FRF to the general form of a single mode's contribution to an FRF. This procedure may be used to replace the non-linear least squares routine previously implemented in AMI.

The complete elimination of non-linear least squares routine represents a significant improvement to AMI, so a new description and evaluation of its performance is in order. The system used for this assessment is the same as the one previously used by Drexel, Ginsberg, and Zaki [4], specifically, a cantilevered beam with three suspended mass-spring-dashpot subsystems, see Figure 1. The subsystem at the end of the beam is tuned so that its natural frequency coincides with the first bending frequency of the beam, so the subsystem at the end acts like a vibration absorber for excitation at that location. This leads to two natural frequencies close to the fundamental frequency of the isolated beam. Further, because the other two subsystems are detuned from the isolated beam's natural frequencies, these subsystems give rise to modes that are poorly excited by an excitation of the beam.

The damping is light, yet non-proportional, and sufficient to cause the closely spaced modes' resonant peaks to merge, which is the phenomenon of mode coupling. The response data for the trial is derived analytically by solving the (state-space) modal differential equations for the impulse response, to which a significant level of white noise is added. FFT processing of the noise contaminated impulse responses yields the complex frequency response data that is input to AMI.

THE BASIC ALGORITHM

The Algorithm of Mode Isolation (AMI) is a SIMO (single-input-multi-output) or MISO, technique for extracting modal properties from frequency domain response data. A brief description follows. For more details see [4] and [6]. The steady-state response of a linear system to a set of generalized forces at frequency ω with complex amplitudes Q_n is given by

$$q_j = \mathrm{Re} \sum_{n=1}^{N} G_{jn}(\omega) Q_n \exp(i\omega t) \tag{1}$$

The raw data for AMI is the set of j displacement FRFs G_{jP} generated by excitation at the Pth location over a range of frequencies. By reciprocity, $G_{jP} = G_{Pj}$, so the data may also be extracted by measuring the displacement at a fixed location P resulting from excitation at a multitude of locations j. These response functions may be expressed in terms of the properties of complex modes associated with a state-space description, see Ginsberg [9]. It is assumed that all modes are underdamped, corresponding to eigenvalues that occur as complex conjugate pairs according to

$$\lambda_k = -\zeta_k \omega_k \pm i\omega_k \sqrt{\left(1-\zeta_k^2\right)} \tag{2}$$

where ω_k and ζ_k are the undamped natural frequency and damping ratio for mode k,

$$\omega_k = |\lambda_k|\,, \quad \zeta_k = -\,\mathrm{Re}\,(\lambda_k) \,/\, |\lambda_k| \tag{3}$$

Each FRF may be described as a sum of contributions of individual modes, with the individual terms described by a pole and a residue. A series of manipulations based on the conjugate properties of the complex modes [4] reveals that

$$\begin{aligned} G_{jP}(\omega) &= \sum_{k=1}^{N} G_{jPk}(\omega) \\ G_{jPk}(\omega) &= \frac{A_{jk}^{(1)} + iA_{jk}^{(2)}}{i\omega - \lambda_k} + \frac{A_{jk}^{(1)} - iA_{jk}^{(2)}}{i\omega - \lambda_k^*} \end{aligned} \tag{4}$$

where $A_{jk}^{(1)}$ and $A_{jk}^{(2)}$ are residue coefficients associated with the pole at $i\omega = \lambda_k$. These constants depend solely on the eigensolution for mode k,

$$\begin{aligned} A_{jk}^{(1)} &= \mathrm{Re}\,(\lambda_k \Phi_{jk} \Phi_{Pk}) \\ A_{jk}^{(2)} &= \mathrm{Im}\,(\lambda_k \Phi_{jk} \Phi_{Pk}) \end{aligned} \tag{5}$$

A full application of the AMI algorithm requires a set of FRFs $G_{jP}(\omega)$ spanning a range of frequencies for a specified drive point P and all measured response points j. Each data set for a specified pair of indices j and P forms a complex vector that is processed individually by AMI in the first two of a three phase process. In the Subtraction Phase, initial estimates for the properties of each mode are obtained by a single-degree-of-freedom (SDOF) technique. This entails matching the largest peak in the FRF to the contribution of a single mode. As each estimate is found, it is used to subtract that mode's contribution from the FRF, thereby making the next most significant mode appear to have the largest contribution. This process continues until the FRF has been reduced to noise. Prior to AMI, Ewins [10] and

Maia *et al* [11] had also suggested these subtraction operations without any further steps. However, terminating processing at this stage fails to recognize that other modes might contribute significantly in the vicinity of a specific mode's resonance. This is especially the case when mode coupling occurs, for then the difference of natural frequencies is comparable to the individual mode's bandwidth.

The Isolation Phase compensates for these overlapping contributions. Here, the current estimates for each mode's properties are used in an iterative process to improve the estimate for each mode. These operation entail sequentially bringing each mode into focus by subtracting the contributions of the other modes to the FRF data. Performing an SDOF fit on the isolated FRF yields an improved estimate for the isolated mode's properties. Isolation of each mode continues until convergence criteria for the modal properties are satisfied. The eigenvalues from all j FRFs are then averaged resulting in a set of N eigenvalues for the system. The Global Mode Vector Phase uses the identified eigenvalues to fit all FRFs to the standard form given by eq. (4). This last phase was the primary innovation introduced by Zaki [5]. A detailed description of these operations follows.

Subtraction Phase

The first phase begins by using the original $G_{jP}(\omega)$ data set to obtain estimates for the most dominant mode's eigenvalue λ_1 and residue coefficients $A_{j1}^{(1)}$ and $A_{j1}^{(2)}$.The first estimated mode's eigenvalue and residue coefficients are used to form G_{jP1} at each frequency according to the second of eqs. (4). This forms a "subtraction residual FRF" that is then used to estimate the next most dominant mode's properties. To place these steps in an analytical framework let $Y_j^{(k)}(\omega)$ denote the subtraction residual after modes 1 to k have been subtracted. Then the successive subtraction residuals are computed according to

$$\begin{aligned} Y_j^{(0)}(\omega) &= G_{jP}(\omega) \\ Y_j^{(k)}(\omega) &= Y_j^{(k-1)}(\omega) - G_{jPk}(\omega) \end{aligned} \tag{6}$$

where $G_{jPk}(\omega)$ is computed by substituting the kth mode's properties into the second of eqs. (4). Each subtraction residual $Y_j^{(k)}(\omega)$ in the frequency range of its maximum magnitude is fit to the form in the second of eqs. (4) in order to identify the values of λ_k, $A_{jk}^{(1)}$ and $A_{jk}^{(2)}$ corresponding to that peak. Previous work used a non-linear least squares approach to fit the data, but this is replaced in the present work with the recent linear least squares procedure [8]. A summary of this procedure will be provided after the AMI operations have been discussed.

The subtraction process continues until the residual FRF contains no identifiable mode. Recognition of this condition presently is achieved by visual inspection of Bode and Nyquist plots of the residual FRF. The preliminary estimate for the number of modes is taken to be the number of subtraction steps carried out in this first phase.

Isolation Phase

The general concept of "isolating" a mode involves using the current estimates of the other modes' parameters to subtract their contribution from the FRF data. If those estimates were exact and noise were not present in the data, what remains after subtraction would be the isolated mode. When the parameters of that mode are identified by the single mode identification scheme used in the Isolation Phase, the results should be more accurate because the data that is processed does not contain the contributions of other modes. Let $X_j^{(n)}(\omega)$ denote the "isolation residual" data set for displacement j when mode n is in focus. By definition this data set is computed by subtracting from $G_{jP}(\omega)$ the contributions of all modes except mode n,

$$X_j^{(n)}(\omega) = G_{jP}(\omega) - \sum_{\substack{k=1 \\ k \neq n}}^{N} G_{jPk}(\omega) \tag{7}$$

where the $G_{jpk}(\omega)$ at each frequency are found by substituting into eq. (4) the current estimates of modal parameters obtained from previous operations. The $X_j^{(n)}$ data set is processed to estimate λ_n, $A_{jn}^{(1)}$, and $A_{jn}^{(2)}$. Because the data now is dominated by a single mode, the result should be improved estimates. As was the case for the subtraction phase, the modes are isolated in the sequence of their contribution to the FRF data.

Because the identification of the other modes is not exact and noise is present, an isolation residual contains the errors due to misidentification of the modes that are not in focus, as well as the noise. Consequently, the isolated mode also is not identified exactly. An iterative process progressively reduces identification errors. A full isolation step processes all modes according to eq. (7), until $n = N$. The sequence is repeated until convergence criteria for the modal parameters are met. Iterating until the real and imaginary parts of each eigenvalue change by less than 0.01% yields good results. For moderately coupled modes only four to five iterations are typically required. Many more iterations may be necessary if a pair of modes are closely coupled.

After a convergent set of parameters have been obtained, it is possible to test whether the number of identified modes N is correct. To do so, a subtraction residual $Y_j^{(N)}(\omega)$ is formed according to the second of eqs. (6) using the convergent set of modal parameters. If this subtraction residual appears to contain coherent artifacts of a mode, the data is processed by the single mode identification scheme, the value of N is incremented, and the newly identified modal

parameters are combined with the values already obtained to restart the isolation phase.

Global Mode Vector Phase

Theoretically, processing the data set for coordinate q_j as described in the preceding would give an estimate of λ_k for $k = 1, ..., N$. It would also yield an estimate of the coefficients $A_{jk}^{(1)}$ and $A_{jk}^{(2)}$ for that specific j (coordinate) and all k (modes). Subjecting each displacement data set to the same processing in such ideal circumstances would lead to multiple estimates of the natural frequencies, and a single estimate of the set of $A_{jk}^{(1)}$ and $A_{jk}^{(2)}$ coefficients. The normalized eigenvectors would then be calculated by solving eqs. (5),

$$\begin{aligned} \Phi_{Pk} &= \left(\frac{A_{Pk}^{(1)} + iA_{Pk}^{(2)}}{\lambda_k} \right)^{1/2} \\ \Phi_{jk} &= \left(\frac{A_{jk}^{(1)} + iA_{jk}^{(2)}}{\lambda_k \Phi_{Pk}} \right), \quad j \neq P \end{aligned} \tag{8}$$

The difficulty with this procedure is that it requires that each mode be identified at the drive point P, so that the factors $A_{Pk}^{(1)}$ and $A_{Pk}^{(2)}$ are known. In practice, some modes might not be identified at the drive point, either because the modal force is small, or because the mode's contribution to the FRF is masked by noise. This may be remedied by discarding the residue factors obtained from the Isolation Phase. Instead, corresponding eigenvalues obtained from each FRF are averaged, then used to perform a global fit of the FRF data for each displacement j to the standard form given by eq. (4).

Let Ω_m denote a set of frequencies in the vicinity of each natural frequencies. Only the FRF data at these frequencies is used for the global fit, because the signal to noise ratio should be the highest there. A total error residual is formed by subtracting from the FRF at each Ω_m the model equation for that FRF, and then adding the differences,

$$R_j = \sum_m \left[G_{jP}(\Omega_m) - \sum_{k=1}^{N} \left(\frac{A_{jk}^{(1)} + iA_{jk}^{(2)}}{i\Omega_m - \lambda_k} + \frac{A_{jk}^{(1)} - iA_{jk}^{(2)}}{i\Omega_m - \lambda_k^*} \right) \right] \tag{9}$$

Because the eigenvalues have been set, the only unknowns in this residual are the $A_{jk}^{(1)}$ and $A_{jk}^{(2)}$ coefficients, which occur linearly. A merit function of these unknown coefficients is formed by decomposing R_j into its real and imaginary parts and then summing the squares. A linear least squares procedure, as described by Chapra [12], leads to the desired values. The $A_{jk}^{(1)}$ and $A_{jk}^{(2)}$ that have been determined are then substituted into eqs. (8) in order to determine the mode vectors.

It should be noted that this procedure leads to identification of *all* $A_{jk}^{(1)}$ and $A_{jk}^{(2)}$ coefficients, even if a mode was not identified when some of the FRF data was processed in the subtraction and isolation phases. This means that the outcome will be estimation of all normal modes, which would seem to overcome the aforementioned difficulty of low drive point mobility in a mode. Such thinking can be deceptive. If the contribution of a particular mode k at the drive point is significantly below the noise threshold, the value of $G_{PP}(\Omega_m)$ in the region where Ω_m is close to $\mathrm{Im}(\lambda_k)$ will reflect the mean noise amplitude, rather than the true contribution of that mode. Such a situation will lead to substantial error in calculation of Φ_{Pk}, and hence of all Φ_{jk}. In this case the overall proportions of the mode vector will be correct for any coordinates whose FRF values in this frequency range are above the noise level, although the mode will not be accurately normalized.

Single Mode Parameter Identification

A key operation for both the Subtraction and Isolation Phases is fitting of the FRF data to the form of a single mode in order to estimate an eigenvalue and associated residue coefficients. A linear least squares procedure for carrying out this task was offered by Ginsberg, Allen, and Ferri [8]. Its highlights will be presented here for the sake of completeness. The first step is to consider the FRF to consist of a single mode, represented by rationalizing the second of eqs. (4). This gives

$$G_{jP}(\omega) = 2\frac{[i\omega - \mathrm{Re}(\lambda_k)] A_{jk}^{(1)} - \mathrm{Im}(\lambda_k) A_{jk}^{(2)}}{|\lambda_k|^2 - \omega^2 - 2i\omega\,\mathrm{Re}(\lambda_k)} \tag{10}$$

Clearing the denominator in eq. (10) and breaking the result into real and imaginary parts then leads to

$$\begin{aligned} \mathrm{Re}[G_{jP}(\omega)] \left(|\lambda_k|^2 - \omega^2 \right) + 2\omega\,\mathrm{Im}[G_{jP}(\omega)]\,\mathrm{Re}(\lambda_k) \\ = -2\left[\mathrm{Re}(\lambda_k) A_{jk}^{(1)} + \mathrm{Im}(\lambda_k) A_{jk}^{(2)} \right] \end{aligned} \tag{11}$$

$$\begin{aligned} \mathrm{Im}[G_{jP}(\omega)] \left(|\lambda_k|^2 - \omega^2 \right) - 2\omega\,\mathrm{Re}[G_{jP}(\omega)]\,\mathrm{Re}(\lambda_k) \\ = 2\omega A_{jk}^{(1)} \end{aligned} \tag{12}$$

Both equations are linear in the four variables $|\lambda_k|^2$, $\mathrm{Re}(\lambda_k)$, $A_{jk}^{(1)}$, and $\left(\mathrm{Re}(\lambda_k) A_{jk}^{(1)} + \mathrm{Im}(\lambda_k) A_{jk}^{(2)} \right)$. If this pair of real equations are evaluated at two arbitrary frequencies, the result is four linear simultaneous equations that may be solved for the unknowns. Once those quantities are determined, the values of $\mathrm{Im}(\lambda_k)$ and $A_{jk}^{(2)}$ are readily extracted. In practice, evaluation of eqs. (11) and (12) at two frequencies is not sufficient, because the values of $G_{jP}(\omega)$ contain the contribution of more than one mode, and also because these values are contaminated with noise. Consequently, the four combination variables are determined by

evaluating the equations at a multitude of frequencies, and then solving them in a least squares sense.

Selecting which frequencies to use for the least squares solution leads to a dilemma because the best signal-to-noise ratios are at the resonance peaks. If the least squares solution uses many frequencies far from a resonance, the corresponding $G_{jP}(\omega)$ might differ significantly from the true value, thereby enhancing the error of the identification. However, if too few frequencies are used (the minimum is two), there will be little opportunity for the least squares computation to minimize the effect of noise. This dilemma was resolved by Ginsberg, Allen, and Ferri [8] through a detailed Monte Carlo study. They found that using all FRF points above the quarter-power points gave the best results for uniformly distributed random noise at several levels. This criterion is met by selecting for the least-squares fit only those values of $G_{jP}(\omega)$ that satisfy $|G_{jP}(\omega)| \geq \delta \max(|G_{jP}(\omega)|)$, where $\delta = 0.5$ yields the quarter-power points.

TUNED VIBRATION ABSORBER

The system and its analysis was described in detail by Drexel, Ginsberg, and Zaki [4]; a brief summary is repeated here. The system consists of a steel cantilever beam, with three spring-mass-damper systems attached to it at $x_1 = L/2, x_2 = 3L/4, x_3 = L$, measured from the support point as shown in Figure 1. The beam has a modulus of elasticity $E = 207$ GPa, density $\rho = 7800$ kg/m^3, second moment of area $I = 3.125\left(10^{-7}\right)$ m^4, cross sectional area $A = 0.0015$ m^2, and length $L = 2$ meters. The natural frequencies of the isolated beam without attachments are denoted as $\hat{\omega}_n$; the fundamental frequency is $\hat{\omega}_1 = 65.3594$ rad/s. The parameters of the attached

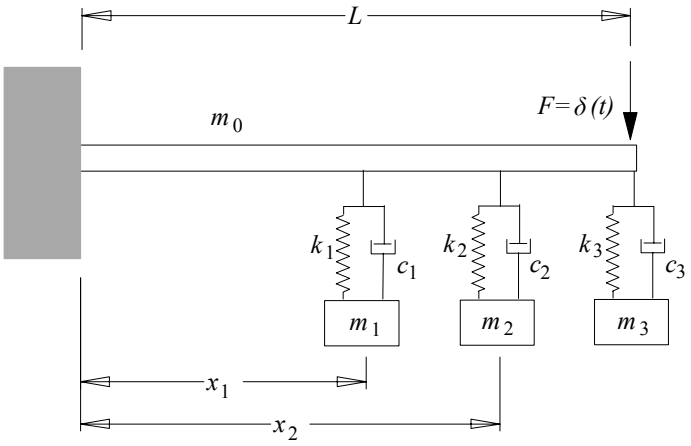

Figure 1: Cantilever beam with attached subsystems.

subsystems are defined such that their stiffnesses k_j are equal, their fixed-base natural frequencies Ω_j increase linearly, and their fixed-base damping ratios are constant at ζ. Thus, the jth spring-mass-damper system is described by $k_j = \sigma\rho AL\hat{\omega}_1^2$, $m_j = k_j/\Omega_j^2$ and $c_j = 2\zeta(k_j m_j)^{1/2}$, where $\sigma = 0.0001$, $\Omega_j = [30.5555 \quad 48.0392 \quad 65.5228]$ rad/s, and $\zeta = 0.015$ for this example. The FRFs processed by AMI are the beam displacement at the end, where the excitation is applied, and the displacements of the three subsystems.

This system was chosen because it exhibits some of the phenomena that typically cause difficulty for mode identification algorithms. The attachment at the end of the beam is tuned such that its natural frequency matches the fundamental frequency of the beam. This subsystem acts as a vibration absorber, whose split natural frequencies are closely spaced as a consequence of the smallness of the suspended mass m_3. The dashpot constant c_3 is adjusted such that the bandwidth of the closely spaced modes is comparable to the frequency difference. Furthermore, because the other subsystems have low mass, and are detuned relative to the beam and the farthest subsystem, the drive point mobility at the natural frequencies of those subsystems is extremely low.

To represent the coupled response of the beam and the subsystems, the beam displacement is described by an Ritz series having J terms,

$$w(x,t) = \sum_{j=1}^{J} \Psi_j(x) q_j(t) \tag{13}$$

The mode functions of the isolated clamped-free beam are used as the basis functions, so

$$\begin{aligned} \Psi_j(x) = \quad & \sin(\alpha_j x) - \sinh(\alpha_j x) \\ & -R_j * (\cos(\alpha_j x) - \cosh(\alpha_j x)) \\ R_j = & \left(\frac{\sinh(\alpha_j) + \sin(\alpha_j)}{\cosh(\alpha_j) + \cos(\alpha_j)}\right) \\ & \cos(\alpha_j)\cosh(\alpha_j) = -1 \end{aligned} \tag{14}$$

The number of degrees of freedom is $J + 3$. Using the Ritz series to construct the mechanical energies and power dissipation leads to mass, stiffness, and damping matrices. The first four natural frequencies of the system are $\omega_k = 30.6, 48.03, 65.0, 65.90$ rad/s, and the respective damping ratios are $\zeta_k = 0.015, 0.015, 0.006, 0.009$. (The fifth and higher modes are the second and higher modes of the beam, with no significant displacement of the attached subsystems.)

The response of the system to an impulsive force at the end of the beam is constructed using a damped modal solution to the equations of motion. This involves solving a symmetric eigenvalue problem associated with the state-space form of the equations of motion, which accounts for nonproportional damping without approximation [9]. That transformation leads to $J + 3$ uncoupled first order differential equations for the modal coordinates, accompanied by $J + 3$ corresponding complex conjugate equations that need not be solved explicitly. The modal impulse responses

have the form $C_k \exp(\lambda_k t)$ with participation factors C_k that depend on the modal coefficients for the drive point. Retracing the modal transformation leads to the time responses of the Ritz series coefficients and the positions of the masses. For the present analysis, the displacement at the tip of the beam, as well as the displacements of the attached masses were collected to form the generalized coordinate vector $\{y(t)\} = [w_L \ w_1 \ w_2 \ w_3]^T$ for the experiment, where w_L is the displacement of the tip of the beam and w_1,w_2, and w_3 are the vertical displacements of the attached masses. Because the excitation is applied at the end of the beam, $P = 1$, so the FRFs to be processed by AMI are $G_{j1}(\omega)$.

It is important that the analysis simulate a properly implemented experiment. This requires selection of the sampling rate and the time window. Based on the minimum modal decay constant $-\mathrm{Re}(\lambda_k)$, a 60 second time window was chosen to eliminate leakage. The corresponding frequency increment is 0.1047 rad/s, which is much less than the bandwidth $2\zeta_k\omega_k$ for the lowest four modes, as well as the difference between the proximate natural frequencies. The number of samples was taken to be 2^{12}, so that the Nyquist frequency 214 rad/s is much larger than the largest frequency component in the response.

The analytical time-domain data at each instant is contaminated by Gaussian white noise at 15% of the signal amplitude according to

$$y_j(t_n)_{\text{corrupt}} = y_j(t_n) + \alpha \left[\max_n (y_j(t_n))\right] r_{jn} \qquad (15)$$

where $-1 < r_{jn} < 1$ is a uniformly distributed random number, the bracketed term is a diagonal array of maxima, and α is a constant that scales the random value to the required fraction of signal amplitude (0.15 for this case). The contaminated impulse response data for each j is then transformed into the frequency domain by an FFT, which leads to a set of FRFs, $G_{j1}(\omega)$.

Eigenvalue Results

Figures 2 and 3 respectively display the noise contaminated FRF and clean FRF at the end of the beam, $j = 1$, while Figures 4 and 5 convey the corresponding results for the displacement of the suspended mass at $x = 3L/4$. The 3rd and 4th natural frequencies are sufficiently close that at first glance only a single peak is evident in the FRFs. Zooming in on the peak of the noise-free version of $G_{11}(\omega)$ reveals a small dip that suggests the presence of two modes, but that feature is not evident in the noise contaminated data.

The signal to noise ratio at any frequency may be evaluated from the noise contaminated value $G_{j1}(\omega)$ and the analytical value, which may be computed directly in the frequency domain. The ratio at the peaks ranged from 10 dB to 21 dB; the latter was observed in the FRF for the end of the beam, $j = 1$, close to the third and fourth natural frequencies. The averages of the signal-to-noise ratios for each FRF at all frequencies were computed to be 3.1dB, 2.4 dB, 2.4 dB, and 2.6 dB for $j = 1, 2, 3, 4$, respectively.

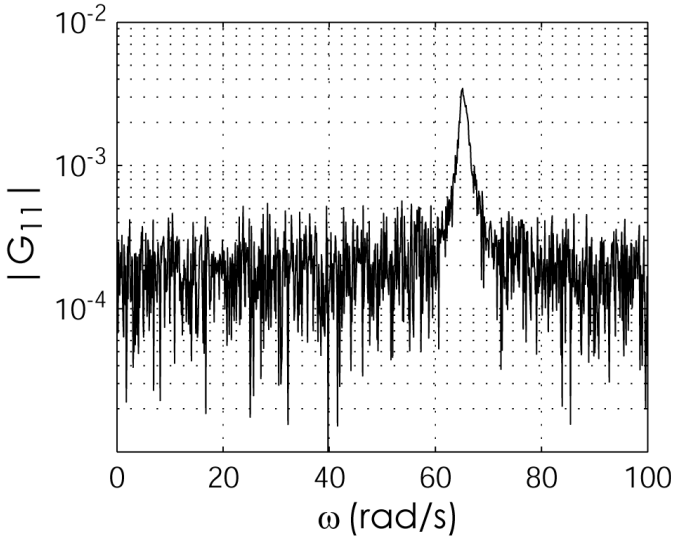

Figure 2: Magnitude of the noise-contaminated FRF for displacement at the end of the beam.

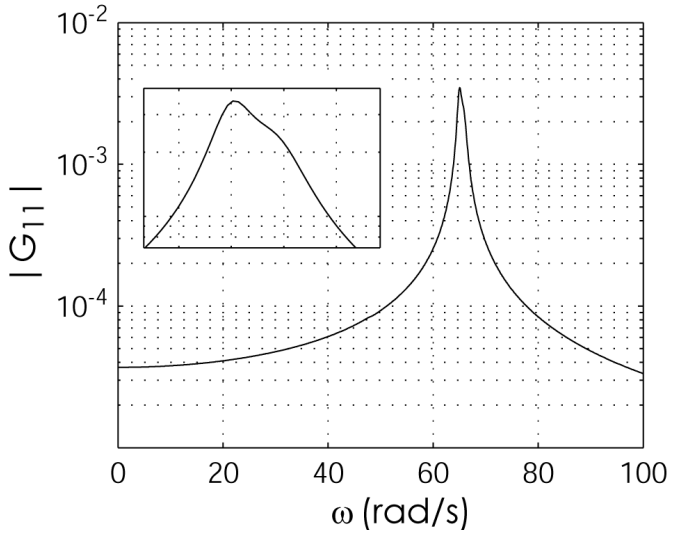

Figure 3: Magnitude of the noise-free FRF for displacement at the end of the beam.

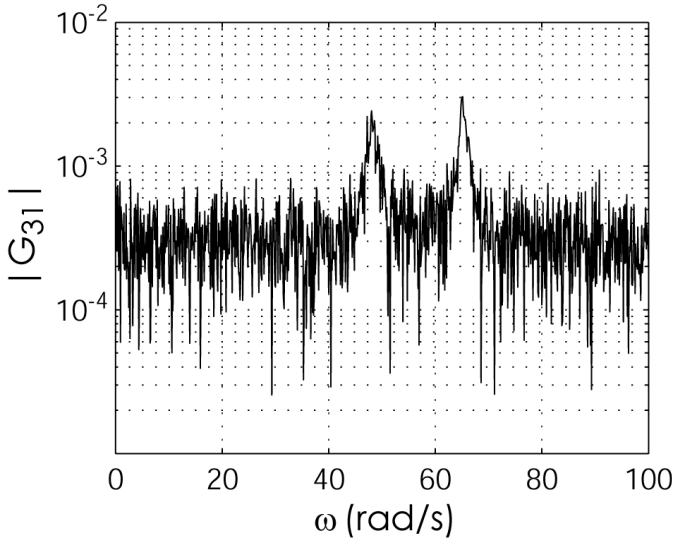

Figure 4: Magnitude of the noise-contaminated FRF for displacement of the suspended subsystem at $x = 0.75L$.

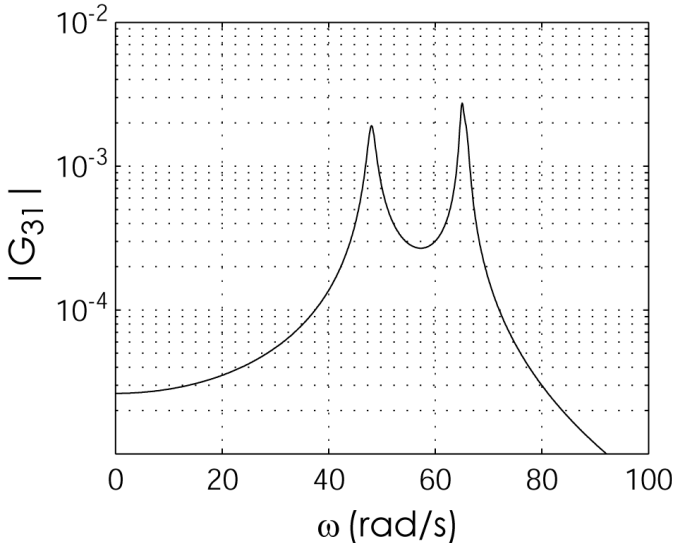

Figure 5: Magnitude of the noise-free FRF for displacement of the suspended subsystem at $x = 0.75L$.

The result of processing the four noise-contaminated FRFs with the Subtraction and Isolation phases of the AMI algorithm was four sets of eigenvalues. Tables 1 and 2 list the values that were obtained. Two or three modes were identified from each G_{j1} data set. An $\times$ in the table indicates that the mode was not detected in the corresponding FRF.

Failure to recognize a mode in a specific FRF may be explained by examining the noise-free FRF data. For example,

Processed data	**Mode 1**	**Mode 2**
G_{11}	$\times$	$\times$
G_{21}	-0.46025+30.555i	$\times$
G_{31}	$\times$	-0.71644+ 48.041i
G_{41}	$\times$	$\times$
Average	-0.46025+30.555i	-0.71644+48.041i
Analytical	-0.45827+30.551i	-0.71973+48.025i
Error (%)	0.43+0.0125i	-0.46+0.0338i

Table 1: Eigenvalues Identified in Each FRF

Processed data	**Mode 3**	**Mode 4**
G_{11}	-0.3513+65.046i	-0.46740+65.803i
G_{21}	-0.48261+65.190i	$\times$
G_{31}	-0.34713+64.983i	-0.57261+65.789i
G_{41}	-0.39469+65.010i	-0.59237+65.915i
Average	-0.39394+65.057i	-0.54413+65.836i
Analytical	-0.39311+65i	-0.59137+65.896i
Error (%)	0.21+0.0880i	-7.99-0.0906i

Table 2: Eigenvalues Identified in Each FRF

Figure 5 for the suspended mass at $x = 3L/4$ shows no indication of a resonance at the fundamental natural frequency, because that mode consists primarily of motion of the first attached subsystem at its fixed-base natural frequency. A similar effect shows up in processing G_{21}, which yielded the least accurate value of λ_3 and no value for λ_4. In essence, the fourth mode's contribution to G_{21} was completely masked by the noise, but its presence adversely affected the identification of mode 3.

The average error is 0.056% in natural frequency and 2.2% in modal damping ratio (2.2% in the real part of the eigenvalue and 0.056 % in the imaginary part.) A few repetitions with various data sets (various random noise sets) showed similar results, suggesting that the results above are typical. Drexel, Ginsberg, and Zaki [4], who employed a nonlinear least squares procedure to perform the single mode parameter identification, reported 0.03% average error in natural frequency and 6% average error in the damping ratio. (The noise-contaminated data used previously was not available, so this is not a perfect comparison.)

Mode Vector Results

The average eigenvalues obtained in the preceding section serve as inputs to the linear least squares routine used to compute the mode vectors. The result of that computation is the set of residue factors $A_{jk}^{(1)}$ and $A_{jk}^{(2)}$ that best fit all FRFs when the eigenvalues are the specified values. The corresponding four normal mode vectors, $k = 1, 2, 3, 4$, are obtained according to eqs. (8). Plots of these vectors lack

	Mode 1-AMI	Mode 1-Analytical
$q_1 \times 10^6$	394.68 + 365.5i	-2.9046 + 93.979i
$q_2 \times 10^6$	-12153 + 10827i	1677.5 +223660i
$q_3 \times 10^6$	521.37 + 392.8i	-1.6448 + 42.909i
$q_4 \times 10^6$	3700.6 - 17657i	-1.7555 + 49.645i

Table 3: Comparison of identified and analytical first mode vectors.

	Mode 2-AMI	Mode 2-Analytical
$q_1 \times 10^6$	211.81 + 375.55i	-17.818 + 308.69i
$q_2 \times 10^6$	-13.136 + 56.514i	2.5513 - 29.414i
$q_3 \times 10^6$	-33957 + 55618i	1682.2 +223650i
$q_4 \times 10^6$	12513 - 10253i	-18.479 + 275.7i

Table 4: Comparison of identified and analytical second mode vectors.

	Mode 3-AMI	Mode 3-Analytical
$q_1 \times 10^6$	919.46 - 4051.3i	3087.1 - 9547.9i
$q_2 \times 10^6$	-113.66 + 388.41i	-148.09 + 371.8i
$q_3 \times 10^6$	-983.9 + 3138.5i	-1204.8 + 3056.2i
$q_4 \times 10^6$	-86751 -146340i	-84362 -152480i

Table 5: Comparison of identified and analytical third mode vectors.

	Mode 4-AMI	Mode 4-Analytical
$q_1 \times 10^6$	1246.7 + 2858.9i	4087.6 + 7212.4i
$q_2 \times 10^6$	-100.92 - 273.44i	-140.6 - 286.58i
$q_3 \times 10^6$	-803.4 - 2149i	-1149.5 - 2284.9i
$q_4 \times 10^6$	47647 -194670i	64054 -194960i

Table 6: Comparison of identified and analytical fourth mode vectors.

resolution, so the identified mode vectors are compared to the analytical values in Tables 3-6. Each analytical mode features dominant displacement of one suspended subsystem, with displacement at the end of the beam being significant only in the third and fourth modes. For the latter modes the dominant terms are quite close to the analytical values.

The overall accuracy of a mode vector may be described by ratioing the Euclidean norm of the difference between the identified and analytical modes to the norm of the analytical modes. The error metrics for mode vectors 3 and 4 are respectively 5.0% and 8.4%. These results are significantly better than those obtained with the original version of AMI, as given by Drexel, Ginsberg, and Zaki [4], where the corresponding errors were 35% and 49%. In contrast, modes 1 and 2 are in error by more than an order of magnitude. These large discrepancies are readily explained by examining the FRFs with and without noise in the context of eq. (9) describing the linear least squares procedure for computing modes. This equation indicates that processing the drive point FRF, $G_{11}(\omega)$ simultaneously yields the residue coefficients $A_{1k}^{(1)}$ and $A_{1k}^{(2)}$ for modes $k = 1$ to 4. Figures 2, and 3 indicate that this FRF is dominated by noise in the range below 50 rad/s, within which the first two natural frequencies lie. Consequently, although the linear least squares routine yields values of $A_{11}^{(1)}$ and $A_{11}^{(2)}$ needed to evaluate Φ_{11}, and values of $A_{12}^{(1)}$ and $A_{12}^{(2)}$ needed to evaluate Φ_{12}, the FRF data that is fit for that computation is random noise. Because these mode coefficients at the drive point are used to scale the modes at all other measurement points, see eq. (8), the result is large scaling errors.

Similar considerations apply for the other FRFs. Least squares processing of $G_{21}(\omega)$ yields the residue coefficients $A_{2k}^{(1)}$ and $A_{2k}^{(2)}$, but $G_{21}(\omega)$ is dominated by noise in the vicinity of the second natural frequency, so $A_{22}^{(1)}$ and $A_{22}^{(2)}$ are unreliable. This compounds the scaling error arising from poor evaluation of Φ_{21}. Similarly, $G_{31}(\omega)$, from which $A_{3k}^{(1)}$ and $A_{3k}^{(2)}$ are obtained, is dominated by noise in the vicinity of the first natural frequency, see Figures 4 and 5. Consequently, the error in $A_{31}^{(1)}$ and $A_{31}^{(2)}$ is increased beyond the scaling error associated with an erroneous Φ_{21}. The case of $G_{41}(\omega)$ is like that of $G_{11}(\omega)$, in the sense that this data also is essentially noise below 50 rad/s. Thus, the values of $A_{41}^{(1)}$ and $A_{41}^{(2)}$ leading to Φ_{41}, and of $A_{42}^{(1)}$ and $A_{42}^{(2)}$ leading to Φ_{42}, lack reliability.

The significant aspect of the preceding discussion is that Tables 1 and 2 indicate that the first two phases of AMI identified the existence of mode 1 solely when $G_{21}(\omega)$ was processed, while mode 2 was detected solely when $G_{31}(\omega)$ was processed. The original version of AMI used the residue coefficients computed simultaneously with the eigenvalues. Consequently, only values of $A_{21}^{(n)}$ and $A_{32}^{(n)}$ would have been found if the original AMI scheme had been followed. This was the approach followed by Drexel, Ginsberg, and Zaki [4], so they failed to obtain the first and second normal mode vectors.

SUMMARY AND CONCLUSIONS

The revised version of the AMI algorithm is a three phase process. The first two are like those described in the prior works, except for modification of the scheme used to fit FRF data to a single mode. The third phase obtains mass-normalized eigenvectors by performing a global linear least-squares fit of an FRF. This fit is achieved by fixing the eigenvalues at the averages obtained from the first two AMI phases.

The efficacy of this revised scheme was evaluated using synthetic data for a cantilever beam with attached vibration absorbers. A Ritz series representation was used to construct an analytical model. The system's parameters

were such that two natural frequencies were separated by a little more than the half power bandwidth. Also, each FRF shows no evidence of a contribution from one or two modes. State space modal analysis was used to uncouple the equations of motion and derive the impulse response to a unit force at the tip of the beam. White noise was added to the time domain impulse response, scaled at 15% of the maximum signal amplitude for each coordinate. The FFT of the unit impulse responses then yielded the FRF for each measurement point. In the frequency domain, the addition of noise resulted in signal to noise ratios that were between 10 dB and 21 dB at the peaks, with an average of approximately 3 dB across the entire frequency range. Visual inspection of the noise contaminated FRFs showed little evidence that two modes were present near 65 rad/s.

The first two phases of AMI yielded average eigenvalues whose average error was 0.056% in natural frequency and 2.2% in modal damping ratio. Four normal modes were then obtained from the newly added third phase of AMI. This led to very good identifications of the third and fourth modes, with error metrics of 5.0% and 8.4%.. Poor identification of the first and second modes was traced to the fact that some of the FRF data used for the global linear least squares fit was dominated by noise in the vicinity of the first and second natural frequencies. The original version of AMI completely failed to obtain these normal modes. In essence, the global least squares fit of an FRF used in the present version of AMI assures that a normal mode vector will be obtained for each eigenvalue. However, the quality of that identification is limited by the quality of the FRF data in the vicinity of each of the modes.

This numerical experiment suggests that AMI is capable of accurate identification of modes, even in the presence of mode coupling. Good estimates of the eigenvalues may be obtained, even if some FRFs are dominated by noise in the vicinity of some natural frequencies. However, high quality estimation of a mode vector requires that the mode's contribution to the FRF be above the noise level in all FRFs. Failure to meet this condition at an undriven point results solely in poor estimation of that element of that mode vector. However, failure to satisfy it at the drive point leads to mis-scaling of all elements of the mode vector. Thus, like any other modal identification algorithm, AMI relies on suitable selection of the drive point, such that all modes of interest are well excited.

ACKNOWLEDGEMENT

This paper is based on work supported under a National Science Foundation Graduate Research Fellowship.

REFERENCES

[1] Doebling, S. W., Alvin, K. F. and Peterson, L. D., 1994, "Limitations of State-Space System Identification Algorithms for Structures with High Modal Density," Proceedings of the 12th International Modal Analysis Conference (IMAC), Honolulu, HA, 633-637.

[2] Drexel, M. V. and Ginsberg, J. H., 2001, "Mode Isolation: A New Algorithm for Modal Parameter Identification," Journal of the Acoustical Society of America, **110**, 1371-1378.

[3] Drexel, M. V. and Ginsberg, J. H., 2001, "Modal Parameter Identification Using State Space Mode Isolation," Proceedings of the 19th International Modal Analysis Conference (IMAC), Orlando, FL.

[4] Drexel, M. V., Ginsberg, J. H. and Zaki, B. R., 2003, "Implementation of the Mode Isolation Algorithm in the State Space," Journal of Vibrations and Acoustics, forthcoming.

[5] Zaki, B. R., 2002, "A Modified Approach to Improve the Robustness of the Algorithm of Mode Isolation." M.S. Thesis, Georgia Institute of Technology, Atlanta, GA.

[6] Zaki, B. R. and Ginsberg, J. H., 2002, "Noise: Is It the Fundamental Limit for Experimental Modal Analysis?" 6th Biennial Conference on Engineering Systems Design and Analysis, Istanbul, Turkey, July 8-11.

[7] Balmès, E., 1996, "Frequency Domain Identification of Structural Dynamics Using the Pole-Residue Parameterization," Proceedings of the 14th International Modal Analysis Conference (IMAC), Dearborn, MI, 540-546.

[8] Ginsberg, J. H., Allen, M. S., Ferri, A. and Moloney, C., 2003, "A General Linear Least Squares SDOF Algorithm for Identifying Eigenvalues and Residues," Proceedings of the 21st International Modal Analysis Conference (IMAC), Orlando, FL.

[9] Ginsberg, J. H., 2001, *Mechanical and Structural Vibrations: Theory and Applications*, Wiley, New York.

[10] Ewins, D. J., 2001, *Modal Testing: Theory, Practice and Applications*, Second Edition, Research Studies Press Ltd., Baldock, Hertfordshire, England.

[11] Maia, N. M. M., Silva, J. M. M, 1997, *Theoretical and Experimental Modal Analysis*. John Wiley & Sons Inc., New York, & Research Studies Press Ltd., England.

[12] Chapra, S. C. and Canale, R. P., 1988, *Numerical Methods for Engineers*, McGraw-Hill, NY.